

1 **Aerosol Specification in Single-Column CAM5**

2  
3  
4  
5 Bereket Lebassi-Habtezion and Peter M. Caldwell

6  
7 Lawrence Livermore National Laboratory

8  
9  
10  
11  
12  
13  
14 February 11, 2015

15  
16  
17  
18  
19  
20  
21 \_\_\_\_\_  
22  
23 *Corresponding author address:* Peter Caldwell, Lawrence Livermore National Lab, PO  
24 Box 808, Livermore CA 94551. *E-mail:*caldwell19@llnl.gov  
25

26 **Abstract**

27           Single column model (SCM) capability is an important tool for general circulation  
28 model development. The SCM mode of version 5 of the Community Atmosphere Model  
29 (CAM5) is shown to handle aerosol initialization and advection improperly, resulting in  
30 aerosol, cloud droplet, and ice crystal concentrations which are typically much lower than  
31 observed or simulated by CAM5 in global mode. This deficiency has a major impact on  
32 stratiform cloud simulations. It has little impact on convective cases because aerosol is  
33 currently not used by CAM5 convective schemes and convective cases are typically  
34 longer in duration (so initialization is less important). By imposing fixed aerosol or  
35 cloud-droplet and crystal number concentrations, the aerosol issues described above can  
36 be avoided. Sensitivity studies using these idealizations suggest that the Meyers et al.  
37 (1992) ice nucleation scheme prevents mixed-phase cloud from existing by producing too  
38 many ice crystals. Microphysics is shown to strongly deplete cloud water in stratiform  
39 cases, indicating problems with sequential splitting in CAM5 and the need for careful  
40 interpretation of output from sequentially split models. Droplet concentration in the GCM  
41 version of CAM5 is also shown to be far too low ( $\sim 25 \text{ cm}^{-3}$ ) at the Southern Great Plains  
42 Atmospheric Radiation Measurement site.

43 **1. Introduction**

44           The Single Column Model (SCM) version of the Community Atmosphere Model  
45 (CAM) is a very important tool for development of model numerics and physics. One  
46 advantage of the SCM is that it is much more computationally affordable, which allows  
47 developers to easily test a wide variety of model changes. Another advantage is that there  
48 exists a large number of standard SCM case studies exist which can be used to evaluate  
49 model behavior in a wide variety of important climate regimes. These case studies  
50 (typically organized by the Global Energy and Water Experiment Cloud System Study  
51 (GCSS) Boundary Layer Cloud Working Group and later by the Global Atmosphere  
52 System Studies (GASS) Panel) are typically based on observations from field campaigns  
53 which provide data for driving the SCM and for evaluating its output (Randall et al.,  
54 2003). Cases tend to focus on a single meteorological phenomenon, which makes them  
55 perfect testbeds for thinking deeply about the processes responsible for model behavior.

56           In the first GCSS intercomparison (Moeng et al., 1996), liquid water path (LWP)  
57 in nocturnal stratocumulus was found to vary by a factor of 5 across large-eddy  
58 simulation (LES) models. The source of this spread could not be identified because  
59 model parameterizations differed so widely. This experience sparked a long tradition of  
60 idealizing aspects of models performing these standard case studies in order to isolate the  
61 source of differences between simulations. In particular, variables normally predicted by  
62 general circulation models (GCMs) are often hard-coded to observed values in these  
63 SCM case studies in order to separate errors due to prediction of these variables from  
64 errors in other parts of the model. By idealizing or specifying aspects of a simulation, the

65 processes responsible for model bias can be illuminated, providing a pathway towards  
66 model improvement.

67 A significant fraction of the uncertainties in climate projections results from the  
68 representation of aerosol (Haywood and Boucher, 2000; Forster et al., 2007). Aerosols  
69 affect climate by directly absorbing and reflecting atmospheric radiation (known as the  
70 direct effect) and by changing cloud optical properties and lifetimes (known as aerosol  
71 indirect effects). As a result, developing aerosol parameterizations has become a high  
72 priority in the climate modeling community.

73 The inclusion of prognostic aerosol in version 5 of CAM (CAM5) has been a  
74 major milestone in its development (Liu et al., 2012; Ghan et al. 2012). Horizontal  
75 advective tendencies are required for prognostic aerosol, however, and these cannot be  
76 calculated from a single column. The SCM case was not considered in the development  
77 of CAM5 aerosol, so horizontal advective tendencies for aerosol are hardcoded to zero  
78 (i.e. advection neither increases or decreases aerosol concentrations) in CAM5-SCM. It  
79 would be straightforward to edit the code to allow aerosol advection in SCM mode to be  
80 specified, but such functionality would be of limited use since observed aerosol advective  
81 tendencies are not typically available for SCM case studies. A bigger problem is that  
82 CAM5-SCM initializes all aerosol mass mixing ratios to zero. As a result, aerosol  
83 concentrations are unrealistically low (compared to observations or GCM simulations) in  
84 SCM runs until surface emissions (specified from observed climatology) loft sufficient  
85 aerosol. Since this process can take several days (e.g. Schubert et al, 1979), SCM case  
86 studies (particularly stratiform cloud studies, which tend to be short) are plagued by  
87 extremely low aerosol. The goal of this study is to test the impact of CAM5-SCM's

88 aerosol treatment for a variety of classic case studies and to evaluate the efficacy of  
89 several potential solutions to the problems induced by unrealistically low aerosol  
90 concentration.

## 91 **2. Methods**

### 92 *2.1 Model Setup*

93 All simulations in this paper were performed using CAM5, which is described in  
94 detail in Neale et al (2012). Briefly, turbulent transport at all model levels in CAM5 is  
95 computed following Bretherton and Park (2009). Stratiform cloud fraction and  
96 condensation/evaporation is computed following Park et al (2014) and stratiform  
97 microphysics is handled according to Morrison and Gettelman (2008) and Gettelman et  
98 al., (2010). Shallow convection follows Park and Bretherton (2009), while deep  
99 convection is parameterized according to Zhang and McFarlane (1995) as modified by  
100 Richter and Rasch (2008). Radiation is calculated using the Rapid Radiative Transfer  
101 Model (RRTMG) radiation scheme (Mlawer et al., 1997). Aerosol are handled by the  
102 three mode simplified modal aerosol model (MAM3; Liu et al., 2012; Ghan et al. 2012)  
103 with accumulation, Aitken, and coarse modes. MAM3 is capable of treating complex  
104 aerosol physical, optical, and chemical processes and simulating aerosol size, mass and  
105 number distributions. The aerosol size distribution is lognormal, and internal and external  
106 mixing between aerosol components is assumed in the model.

107 In SCM mode, a column from the global model is extracted and driven by  
108 prescribed winds and horizontal advective tendencies (Hack and Pedretti, 2000). This  
109 results in an idealized version of the GCM where code related to fluid flow is replaced by  
110 externally-imposed data but the parameterized physics component of the model retains its

111 full complexity. All SCM runs use a timestep of 1200 sec and 30 vertical grid levels  
112 (with ~20 levels in the free troposphere).

113 Most of the simulations described in this paper are SCM runs as described in Sect.  
114 2.3, but we do conduct two 10 yr-long GCM run using the finite-volume dynamical core  
115 at  $1.9 \times 2.5^0$  resolution for comparison. One simulation was done using the default  
116 prognostic aerosol method and the other uses the prescribed aerosol functionality  
117 included in version 1.2 of the Community Earth System Model (CESM). Both GCM runs  
118 were driven by a repeating annual cycle of year 2000 SST, greenhouse gases, and  
119 aerosols. They use an 1800 sec timestep and the same 30 vertical levels used for the SCM  
120 runs.

## 121 ***2.2 Proposed Solutions***

122 As noted in the introduction, a problem with CAM5-SCM is that aerosols are  
123 initialized to zero and horizontal advection of aerosol is not treated realistically. As a  
124 result, aerosol concentrations in SCM runs are much lower than observed or simulated in  
125 GCM runs. In this section we outline 3 possible solutions to the problem of low aerosol  
126 concentration in CAM5-SCM.

127 1. Our first approach (hereafter called FixHydro) is to fix cloud droplet ( $N_d$ ) and ice  
128 crystal ( $N_i$ ) number concentrations at observed values. Because  $N_d$  and  $N_i$  are the  
129 means through which aerosol affects cloud in CAM5, fixing these concentrations is a  
130 simple way to avoid cloud problems due to low aerosol in CAM5-SCM. The  
131 FixHydro approach is attractive because a). These number concentrations are  
132 available for most popular SCM case studies and b). Specifying  $N_d$  and  $N_i$  isolates  
133 biases in the microphysics from biases related to aerosol treatment. Ability to isolate

134 the parameterization responsible for bad behavior is critical for avoiding a model held  
135 together by compensating errors. One downside to FixHydro is that it does not  
136 alleviate clear-sky impacts of low aerosol. This is not a critical problem since clear-  
137 sky effects tend to be small relative to the radiative impact of cloud changes, but it  
138 does motivate our other solutions.

139 2. Our second method (hereafter called PrescAero) uses the new prescribed aerosol  
140 capability included in CESM version 1.2. PrescAero prescribes mass mixing ratios of  
141 aerosol species using mean climatological values for each month of the year for each  
142 grid cell (based on results from a long prognostic aerosol run). By default, prescribed  
143 aerosol values are specified by daily random draws from a lognormal distribution  
144 based on climatological average values. We turn this random sampling off for SCM  
145 because it would make SCM runs irreproducible and occasionally provides very  
146 unusual values which would unnecessarily complicate interpretation of SCM results.  
147 Random sampling is not needed in the tropics but may be required to reproduce  
148 CAM5 polar climate (Jin-Ho Yoon, personal communication 2014), in which case  
149 ensembles of CAM5-SCM runs are probably needed.

150 3. In our last method, we apply observed mixing ratios and size distributions to the  
151 aerosols in MAM3. This method (hereafter named obsAero) makes use of PrescAero  
152 code but imposes observed rather than modeled mass mixing ratios of the different  
153 aerosol species for all the modes. To use this approach, observed values are needed  
154 for the number concentrations of the aerosol mode  $N_j$ , the geometric mean dry radius  
155  $a_{mj}$ , and the geometric standard deviation  $\sigma_j$  of the multimode lognormal aerosol size  
156 distribution given by the following equation (Abdul-Razzak and Ghan, 2000):

157 
$$\frac{dn}{da} = \sum_{j=1}^3 \frac{N_j}{\sqrt{2\pi}\sigma_j} \exp\left\{-\frac{\ln^2\left(\frac{a}{a_{mj}}\right)}{2\ln^2\sigma_j}\right\}, \quad (1)$$

158 where the summation is over all 3 aerosol modes (accumulation, aitken, and coarse).

159 Each of our 3 solutions has advantages and disadvantages. Many case studies lack  
 160 the information necessary for the ObsAero method and some lack  $N_d$  and  $N_i$  information  
 161 needed for the FixHydro approach. For these cases, PrescAero is the only viable option.  
 162 PrescAero is also the best choice if one's goal is to emulate the behavior of the GCM as  
 163 closely as possible (since it uses aerosol values from the full model). But aerosol from  
 164 GCM simulations is often a poor proxy for observed values (both because values at the  
 165 time of observation may differ greatly from climatology and because the model  
 166 climatology may be biased), so fixes based on observed data are more appropriate for  
 167 experiments which will be validated against observations at a particular time and place.

168 The goal of the experiment also plays a critical role in determining which fix is  
 169 best. For example, FixHydro is clearly inappropriate for studying aerosol effects but its  
 170 simplicity makes it optimal for teasing out errors in the microphysics scheme. ObsAero  
 171 and FixHydro methods are useful for testing aerosol activation but not 2-way  
 172 cloud/aerosol interactions. Comparing FixHydro and ObsAero results may be the best  
 173 way to identify whether biases come from aerosol activation or other processes. In short,  
 174 there is no 'best' approach to obtaining realistic aerosol in CAM5-SCM. Our goal in this  
 175 paper is to prove that all 3 methods yield acceptable solutions and are suitable for use as  
 176 appropriate.

177 If one's goal is to study interaction between cloud and aerosol, none of our  
 178 proposed methods are appropriate. It would be relatively straightforward to add another  
 179 SCM option which initializes aerosol to observed or model-specified values and allows

180 the model to ingest horizontal aerosol advective tendencies. We do not do this because  
181 we do not know of any SCM case studies where such information is available, our  
182 personal research plans don't require this functionality, and global simulations with  
183 specified meteorology (e.g. Rasch et al., 1997) already fill this role.

### 184 *2.3 SCM Cases*

185 In order to test aerosol effects over a range of climatologically-important cloud  
186 regimes we analyze results from 4 case studies, each highlighting a different type of  
187 cloud. These cases include drizzling subtropical stratocumulus, mixed-phase Arctic  
188 stratocumulus, maritime shallow convection, and continental deep convection. The  
189 details of these experiments conducted are summarized below.

#### 190 *DYCOMS RF02 Case*

191 Subtropical stratocumulus are important because of all cloud types they have the  
192 biggest impact on the planetary radiation budget (Hartmann et al., 1992), and difficulty in  
193 simulating them is a leading source of uncertainty in climate sensitivity (e.g. Bony and  
194 Dufresne, 2005). Because they are important yet hard to simulate, stratocumulus have  
195 been the focus of a large number of field campaigns. Research Flight 2 of the Second  
196 Dynamics and Chemistry of Marine Stratocumulus field campaign (hereafter DYCOMS  
197 RF02) sampled drizzling stratocumulus off the coast of California during the night of  
198 July 11, 1999. Data from this flight formed the basis for an SCM intercomparison by  
199 Wyant et al (2007; hereafter W07) and an LES intercomparison by Ackerman et al  
200 (2009). Like previous intercomparisons, the SCMs studied varied greatly in their ability  
201 to predict stratocumulus properties. Precipitation was found to play an important role in

202 these simulations by reducing LWP and (to a lesser extent) reducing cloud-top  
203 entrainment.

204 Our experimental configuration (outlined in Table 1) follows the specifications of  
205 W07 with a few exceptions. One difference is that radiation is calculated using RRTMG  
206 instead of the idealized scheme used in W07. We also kept  $u$  and  $v$  for our simulations  
207 constant instead of calculating winds from specified geostrophic wind profiles (which is  
208 reasonable since shear was not important in DYCOMS RF02). While these changes make  
209 our simulations slightly less comparable to the runs in W07, they are simpler to  
210 implement and produce runs which are still realistic enough to be reasonably compared  
211 against observations. We also turn off cloud processes above 700 hPa to prevent ice  
212 formation at the troposphere, which would otherwise occur due to interaction between the  
213 idealized SCM forcing specifications and subgrid variability assumptions in CAM5.  
214 Observed aerosol information (for testing the ObsAero method) were taken from  
215 Ackerman et al. (2009), who assumed aerosol was comprised entirely of sulfate and  
216 chose parameters for the bimodal lognormal distribution (equation 1) in order to have  $N_d$   
217 match the observed droplet concentration value of  $55 \text{ cm}^{-3}$ .

#### 218 *MPACE-B Case*

219 Our second case comes from the Mixed-Phase Arctic Cloud Experiment  
220 (MPACE), which sampled clouds over open ocean near Barrow, AK. We focus  
221 particularly on the portion of this experiment between October 9, 1700 UTC to October  
222 10, 0500 UTC, 2004 (known as MPACE-B), a period when mixed-phase stratocumulus  
223 was observed. This case was the subject of an intercomparison by Klein et al. (2009;  
224 hereafter K09). Most models participating in this intercomparison greatly underestimated

225 the observed LWP because conversion to ice was too efficient. We choose this case  
226 because mixed-phase stratocumulus are very important to the polar surface budget, yet  
227 models (including CAM5) have a hard time simulating these clouds. MPACE-B is  
228 attractive because it includes both liquid and ice processes without being overly  
229 complicated. Our case setup (listed in Table 1) is similar to K09 with a few notable  
230 exceptions. We again specify winds at all levels while K09 advocates nudging winds  
231 below 700 hPa. We nudge thermodynamics variables to initial conditions above 700 hPa  
232 with a timescale of 1 hr while K09 specifications require all variables to be kept at their  
233 initial values above 700 hPa. These changes were again implemented for convenience  
234 and are not expected to have dramatic effects on our simulations.

235 *RICO case*

236 Shallow Convection is another important cloud type with major impact on climate  
237 sensitivity (e.g. Medeiros et al., 2008). To sample this cloud type, we use data from the  
238 Rain in Cumulus over Ocean (RICO) experiment, which was conducted on the upwind  
239 side of the Islands of Antigua and Barbuda during the winter of 2004 (Rauber et al.,  
240 2007). Unlike previous experiments such as the Atlantic Trade Wind Experiment  
241 (ATEX) and Barbados Oceanographic and Meteorological Experiment (BOMEX) which  
242 did little to measure clouds and precipitation, RICO has extensive cloud-related  
243 measurements, which make it useful for studying shallow cumulus clouds and their  
244 precipitation. Unfortunately, cloud data came at the expense of large-scale information,  
245 forcing modeling studies to use idealized composite information which is not directly  
246 comparable to time-evolving observations. vanZanten et al. (2011), hereafter VZ11,  
247 describe the results of an LES intercomparison based on this composite data. An SCM

248 intercomparison was planned (<http://www.knmi.nl/samenw/rico/index.html>) but never  
249 published. Our simulations are a blend between LES and SCM specifications as listed in  
250 Table 1 and described below. One unique aspect of the RICO case is that radiation  
251 tendencies are included in the prescribed large-scale temperature tendency. As a result,  
252 we had to turn off the shortwave and longwave radiation schemes. The case was designed  
253 specifically to be energetically and moisture balanced, and as a result we found we did  
254 not need to use nudging to obtain stable simulations.

#### 255 *ARM95*

256 The last case we consider is an 18 day long simulation of summertime continental  
257 convection spanning July 18 to Aug 3, 1995 at the Atmospheric Radiation Measurement  
258 (ARM) program's Southern Great Plains (SGP) site. We included this case because for a  
259 long time it was the only SCM case that was included in the released version of CAM.  
260 This case is useful because it tests the model's deep convective scheme (which plays a  
261 huge role in determining model climate), yet is extra-tropical so the imposed vertical  
262 velocity assumption of typical SCMs is less problematic (e.g. Sobel and Bretherton,  
263 2000). This case was the subject of an intercomparison of 11 SCMs and one coarse LES.  
264 As reported by Ghan et al., (2000), temporal variability in the models exceeded observed  
265 values. This was interpreted as forcing error since all models behaved similarly. Large  
266 temperature and moisture biases were reported over the simulation unless nudging was  
267 used; we do not use nudging despite this warning because clouds form at all levels during  
268 the simulation and nudging areas with clouds makes it hard to tell whether model physics  
269 or nudging is causing the modeled behavior. Advective forcing was generated by the  
270 State University of New York (SUNY) objective analysis method (Zhang et al. 2001) and

271 surface fluxes were specified with the Doran et al. (1998) surface analysis technique  
272 using the Simple Biosphere (SiB2) model (Ghan et al., 2000). Forcings for this case are  
273 not included in Table 1 because they vary in time (which makes them impossible to  
274 represent compactly in a table). Aerosol and cloud number densities are not available for  
275 this case, so only Default and PrescAero methods were tested.

276

### 277 **3. Results and Discussion**

278 DYCOMS RF02

279 Table 2 shows observed and modeled cloud-related variables averaged during the  
280 last two hours of the six hour DYCOMS RF02 simulations. In addition to  $N_d$  and surface  
281 precipitation (Pr), we include LWP both before and after microphysics was called  
282 ( $LWP_{pre}$  and  $LWP_{post}$ , respectively). These values are different because CAM5  
283 sequentially updates the model state after each parameterization is applied. As described  
284 in Gettelman et al. (2014),  $LWP_{pre}$  is often much bigger than  $LWP_{post}$  because  
285 microphysics tends to deplete cloud water and when it acts in isolation over the long  
286 model timestep a great deal of water can be lost. We also include cloud base,  $z_b$   
287 (computed by identifying the first layer from the bottom with cloud fraction exceeding  
288 0.5, then linearly interpolating between this layer and the one below it to get the exact  
289 height where cloud fraction = 0.5) and cloud top height,  $z_i$  (computed by identifying the  
290 top-most layer with total water mixing ratio  $q_t > 8 \text{ g kg}^{-1}$  and linearly interpolating between  
291 this layer and the one above it to find the exact height where  $q_t = 8 \text{ g kg}^{-1}$ ). Cloud top  
292 entrainment velocity  $w_e - \delta z_i / \delta t - w_s$  was also computed.

293 The Default method underestimated the observed  $N_d$  ( $=55 \text{ cm}^{-3}$ ), while ObsAero  
294 and particularly PrescAero overestimated  $N_d$ . As expected, runs with higher  $N_d$  tend to

295 precipitate less and as a result have higher LWP. LWP computed before microphysics is  
296 too high except for the Default case. Values after microphysics show more variability,  
297 with the Default case being too low and the FixHydro and PrescAero being too high.  
298 Difference between pre- and post-microphysics values illustrate the difficulty of  
299 interpreting output from sequentially-split climate models.

300 Cloud base and cloud top were both slightly higher than observed yet entrainment  
301 was much smaller than observed. This suggests that the prescribed subsidence may be too  
302 weak in this case study. Surface precipitation is too weak when realistic  $N_d$  is used. This  
303 could be due to excessive re-evaporation of precipitation below the cloud base. This is  
304 consistent with the fact that the ObsAero and FixHydro models have the highest below-  
305 cloud base evaporation of precipitation ( $5.85 \times 10^{-5} \text{ g kg}^{-1} \text{ s}^{-1}$  and  $4.45 \times 10^{-5} \text{ g kg}^{-1} \text{ s}^{-1}$ ,  
306 respectively), while the Default and PrescAero have lower values ( $3.62 \times 10^{-5} \text{ g kg}^{-1} \text{ s}^{-1}$   
307 and  $1.33 \times 10^{-5} \text{ g kg}^{-1} \text{ s}^{-1}$ , respectively).

308 Figure 1a shows  $N_d$  profiles of the different aerosol specification cases averaged  
309 over the last two hours of the simulation period. We have also included the 10 year July-  
310 average  $N_d$  profile of the corresponding 3D CAM5 run in which  $N_d$  values were extracted  
311 at the closest grid point to the DYCOMS RF02 location. The specified aerosol SCM  
312 cases show higher  $N_d$  values at the cloud base and slightly lower values at the cloud top.  
313 This is inconsistent with observations, which tend to show constant values throughout the  
314 cloud (e.g. Martin et al, 1994). The Default run show the lowest  $N_d$  values and PrescAero  
315 showed the highest. Low  $N_d$  for the default scheme is expected because it initializes  
316 aerosol to zero (as noted above); aerosol in the default simulation increased over time due  
317 to surface emission (not shown). The 3D model  $N_d$  values are as high as the PrescAero

318 case but the whole profile is shifted towards the surface. Collapsed boundary layers like  
319 this occur when stratocumulus becomes too thin to maintain the turbulence necessary to  
320 support a deep boundary layer. Differences in behavior between the SCM and GCM runs  
321 are unsurprising because the former were initialized to a well-mixed profile and driven by  
322 observed large-scale conditions for a short time period while the latter had 10 yrs to  
323 develop biases and were driven by large-scale conditions from the model itself.  
324 Additionally, SCM runs are nocturnal while GCM runs include both day and night. This  
325 is relevant since solar radiation damps turbulence, reducing boundary layer height (e.g.  
326 Caldwell et al., 2005). The fact that the GCM results look very different from the SCM  
327 results indicates that the source of GCM bias either takes a long time to spin up or is  
328 related to bad large-scale conditions rather than the quick-acting cloud physics  
329 parameterizations. This is useful information because it tells us that GCM biases in this  
330 case can't be solved solely by analyzing SCM runs.

331           Even though stratocumulus are typically thought to be nonconvective,  
332 shallow convection is triggered occasionally in our DYCOMS RF02 simulations. This  
333 detrainment is a major source of  $N_d$  in simulations with low aerosol. Convective  
334 detrainment can create droplets out of thin air because CAM5 convection schemes detrain  
335 cloud droplets at a fixed droplet mean volume radius with no dependence on aerosol at  
336 all. Convection triggers more often in the Default run, perhaps because strong  
337 precipitation due to low  $N_d$  tends to cause more decoupled, convective conditions. In  
338 order to isolate the effect of convective detrainment on  $N_d$  we conducted a set of  
339 sensitivity experiments where convection detrains vapor rather than condensate.  $N_d$   
340 profiles from these experiments are shown in Fig. 1b. This figure reveals that almost all

341 of the droplets in the Default case are created by convective detrainment. Detrainment  
342 plays a secondary but non-negligible role in the PrescAero and ObsAero cases, especially  
343 near the cloud top.

344 Figure 2 shows the temporal evolution of  $LWP_{pre}$  and  $LWP_{post}$  from the  
345 DYCOMS RF02 case. There is large variability of LWP during the first few hours in all  
346 cases, with variability lasting longest and having largest amplitude in the Default run.  
347 ObsAero shows good agreement with observations, while PrescAero and FixHydro LWP  
348 was too high (consistent with its overpredicted  $N_d$  values).

349 In summary, the DYCOMS RF02 case shows strong sensitivity to aerosol  
350 specification. In the Default case, detrainment from shallow convection is a major source  
351 of  $N_d$ , which artificially limits sensitivity to aerosol burden. Interpretation of model LWP  
352 is very sensitive to whether it is sampled before or after microphysics.

### 353 *MPACE-B*

354 Table 3 shows observed and modeled cloud-related variables averaged during the  
355 last four hours of the MPACE-B case. All runs except FixHydro substantially  
356 overestimate the observed  $N_i$  value. Because the Bergeron process efficiently freezes  
357 liquid when  $N_i$  is plentiful, these runs have zero LWP. The FixHydro case, on the other  
358 hand, has reasonable  $N_i$  and LWP, which illustrates the importance of cloud number  
359 densities for obtaining realistic simulations. The cloud layer for FixHydro is of  
360 approximately the right thickness but is slightly too high in the atmosphere. Its surface  
361 precipitation is a bit too high and its IWP is slightly too low.

362 Figure 3 shows height-normalized MPACE-B profiles of liquid water content  
363 (LWC) and ice water content (IWC) including and excluding snow mass as a function of

364 scaled height, before and after micro-physics. This figure is useful for interpreting our  
365 earlier conclusion that LWP=0 for all runs except FixHydro. Fig. 3a shows that all runs  
366 have LWP>0 before microphysics, so the problem is that each microphysics step removes  
367 all LWC in these runs. LWC before microphysics is, however, underpredicted and cloud  
368 top is too shallow for these runs. This is unsurprising since in mixed-phase  
369 stratocumulus, radiative cooling of liquid at cloud top is the main source of boundary-  
370 layer turbulence (which is needed to supply the cloud layer with liquid and to maintain  
371 cloud top height in the face of subsidence) and radiative transfer in CAM5 is computed  
372 after microphysics (at which point LWP is zero in these runs). In contrast with LWC, all  
373 runs showed reasonable agreement with observations for IWC except FixHydro, which is  
374 a bit higher than the bulk of the observational data (Fig 3b and c). IWC consists,  
375 however, almost entirely of snow for all cases (Fig. 3d). Underprediction of liquid and  
376 dominance of ice over cloud ice have been reported previously for CAM5 (e.g.  
377 Gettelman et al., 2010, Liu et al., 2011).

378         Figure 4 shows the  $N_i$  profiles for all runs averaged over the last four hours of the  
379 MPACE-B period along with the climatological October average  $N_i$  profile from our  
380 GCM run using data from the grid point closest to the MPACE-B location. All SCM runs  
381 except FixHydro have very similar  $N_i$  profiles. This is because ice nucleation at the  
382 temperatures sampled during MPACE-B occurs primarily through  
383 deposition/condensation freezing which is treated in CAM5 by a scheme (Meyers et al.,  
384 1992) which depends only on temperature and saturation vapor pressure. Compared to  
385 the observed value used by FixHydro, all other SCM runs and the GCM overpredict  $N_i$ .  
386 This is a well-known model deficiency which is improved by newer nucleation

387 parameterizations (e.g., Liu et al., 2011, Xie et al., 2013; English et al., 2014).  $N_d$  is not  
388 shown because its cloud-layer average is zero for all cases except FixHydro (where it is  
389 set to the observed value of  $50 \text{ cm}^{-3}$ ; see Table 3).

390 Profiles of cloud fraction are shown in Fig. 5. Interestingly, simulated cloud  
391 *fraction* compares well with aircraft and remote sensing observations for all SCM cases.  
392 Clouds with volume but no mass (commonly called 'empty clouds') were a problem with  
393 CAM3 and CAM4 (e.g. Hannay et al., 2009, Medeiros et al., 2012) because cloud  
394 fraction and condensation/evaporation schemes were disconnected. This disconnect was  
395 patched in CAM5 (Park et al, 2014) so finding empty clouds in this study was somewhat  
396 surprising. The empty clouds seen here for Default, PrescAero, and ObsAero come from  
397 cloud fraction being computed before microphysics and left unchanged even after  
398 microphysics removes all condensate. Closer coupling between cloud fraction,  
399 condensation/evaporation, and microphysics are needed to solve this problem.

400 *RICO*

401

402 Table 4 shows  $N_d$ , surface sensible heat flux (SHF), surface latent heat flux  
403 (LHF), cloud base mass flux (CBMF), cloud cover (the fraction of the sky which appears  
404 to a surface observer to be obscured by clouds), and LWP averaged over the last four  
405 hours of the 24 hour simulation of the RICO case for the four SCM simulations. We  
406 include LES intercomparison data from VZ11 as a crude proxy for truth here because (as  
407 discussed in Sect. 2.3), the RICO case study is created by compositing 2 months of  
408 observations and thus is not comparable with observations from any particular time. SCM  
409 behavior is almost identical for all runs even though aerosol and  $N_d$  vary substantially.

410 This is because clouds in RICO are generated by the shallow convection scheme and (as  
411 mentioned in Sect. 3a) CAM5 convection schemes have no dependence on aerosol.

412 All SCM configurations overestimate the SHF, LHF, and CBMF relative to LES  
413 values but nonetheless capture cloud cover and LWP very well. Similar to DYCOMS  
414 RF02 results, LWP shows high temporal variability at the beginning of RICO SCM  
415 simulations which settles out over time (Fig. 6). Consistent with overpredicted CBMF,  
416 cloud base condensate is overpredicted (Fig. 7a). As expected from previous studies (e.g.  
417 Siebesma et al., 2003), both condensate and mass flux decrease with distance above  $z_b$   
418 (Fig. 7). Fig. 8 breaks cloud cover into its vertical distribution (total cloud fraction) as  
419 well as cloud fraction contributions from shallow, deep, and large-scale contributions.  
420 Even though cloud *cover* is well predicted, cloud *fraction* is overpredicted by the SCMs  
421 because the maximum-random cloud overlap assumption used by CAM5 is inconsistent  
422 with cloud tilt and life-cycle effects found in real shallow convective conditions (Park  
423 and Bretherton, 2009). At cloud base, overestimation is due to both shallow convective  
424 and stratiform clouds. Modeled cloud extends further into the troposphere than observed  
425 due to the deep convection scheme.

426 *ARM95*

427 As noted above, ARM95 is much longer in duration than our other case studies.  
428 During the first 10 simulated days, a large-scale stationary upper-level trough sat over the  
429 continental U.S., resulting in temporally-variable cloud cover and precipitation. There  
430 followed a 3 day period of high pressure and clear skies, and the final 7 days consisted of  
431 stormy weather with high cloud cover and intense precipitation. As noted above, only the

432 Default and the PrescAero cases are simulated due to lack of observed  $N_d$ ,  $N_i$ , and aerosol  
433 data.

434 Figure 9 shows the time series of LWP and IWP for the Default and PrescAero  
435 cases. Observed LWP from Xu and Randall (2000) are also included. SCM runs capture  
436 the observed temporal trends but generally overestimate LWP. Default and PrescAero  
437 behave very similarly, which is consistent with our finding from RICO that aerosol is not  
438 important for convective cases.

439 Fig. 10 shows  $N_d$  profiles from our simulations. Surprisingly,  $N_d$  is fairly similar  
440 for both SCM simulations even though visible aerosol optical depth differs substantially  
441 between these runs (0.163 for PrescAero and 0.081 for the Default case). Typical  
442 observed  $N_d$  values at SGP are around  $200 \text{ cm}^{-3}$  (Frisch et al, 2002; Iacobellis and  
443 Somerville, 2006), so modeled values have a large low bias. Is this a problem with the  
444 SCM setup? We test this by including climatological July data for the GCM grid cell  
445 closest to SGP. We include GCM data from runs using both prognostic and prescribed  
446 aerosol. Both GCM runs show similarly low  $N_d$  values, indicating that this bias is related  
447 to aerosol values predicted by MAM3 rather than the specified values used for the  
448 prescribed aerosol mode. This bias has little impact on model behavior in the current  
449 version of CAM (because convection is independent of aerosol) but may cause problems  
450 in future model versions with more sophisticated convective microphysics.

#### 451 **4. Summary and Conclusions**

452 This study points out that aerosol treatment in CAM5-SCM is unrealistic and  
453 causes problems for non-convective case studies. The issue is that initial aerosol and  
454 horizontal aerosol advective tendencies are hard-coded to zero in SCM mode. Aerosol

455 can still build up in the boundary layer from surface emissions, but the resulting aerosol  
456 loading is likely to be unrealistic because remote sources cannot be included.  
457 Additionally (and more important), SCMs are typically run for a shorter period than it  
458 takes to build up reasonable aerosol concentrations via surface emission and subsequent  
459 lofting into the cloud layer.. As a result, aerosol in SCM runs is typically much lower  
460 than observed or simulated by the GCM. This limits the usefulness of the SCM for model  
461 development.

462 To fix this problem, we propose 3 idealizations: prescribing aerosol from CAM5  
463 climatological values (PrescAero), prescribing aerosol from observations (ObsAero), and  
464 prescribing cloud droplet and ice crystal numbers (FixHydro). We test these  
465 configurations against the default SCM (Default) for 4 different cloud regimes:  
466 summertime mid-latitude continental convection (ARM95), shallow convection (RICO),  
467 subtropical drizzling stratocumulus (DYCOMS RF02), and mixed-phase stratocumulus  
468 (MPACE-B).

469 These fixes were found to have a big impact on non-convective cases. Aerosol  
470 and cloud number density has almost no effect on convective cases, however, because  
471 CAM5 convection does not depend on aerosol or droplet number. Cloud droplet number  
472 at the site of the ARM95 case was found to be underpredicted in CAM5-GCM by a factor  
473 of 8 relative to observations. Even though this deficiency has no effect on CAM5  
474 simulations, lack of dependence on aerosol or droplet number is unrealistic and will be  
475 fixed in future versions of CAM, which makes finding solutions to droplet number  
476 underprediction at SGP worth pursuing even if it doesn't affect the current model version.

477           Shallow convection is found to be unexpectedly triggering in DYCOMS RF02,  
478 where it artificially increases  $N_d$  because convectively-detrained condensate is partitioned  
479 into droplets according to an assumed volume-mean radius rather than a dependency on  
480 available cloud condensation nuclei. Another finding is that the Meyers  
481 deposition/nucleation freezing scheme in CAM5 is too active in the temperature and  
482 moisture conditions sampled during MPACE-B. As a result, ice crystal number  
483 concentration is too high in all of our SCM and GCM runs except FixHydro (which fixes  
484  $N_i$  at observed values). When observed  $N_i$  is used, LWP matches observations. Otherwise  
485 microphysics depletes all liquid water whenever it is called. This results in 'empty clouds'  
486 which have volume but no mass. This trouble with the Meyers et al (1992) scheme has  
487 long been recognized and alternative parameterizations have been explored (e.g., Liu et  
488 al., 2011, Xie et al., 2013; English et al., 2014).  
489

490 **5. Acknowledgements**

491           We thank the Lawrence Livermore National Laboratory (LLNL) for providing  
492 funding through the Multiscale Scientific Discovery through Advanced Computing  
493 (SciDAC) project. The research was performed under the auspices of the United States  
494 Department of Energy by Lawrence Livermore National Laboratory under contract DE-  
495 AC52-07NA27344.

496

497 **6. References**

498

499 Abdul-Razzak, H., and S. Ghan, 2000: A parameterization of aerosol activation: 2.

500 Multiple aerosol types, *J. Geophys. Res.*, **105(D5)**, 6837–6844.

501 Ackerman, A. S., et al., 2009: Large-eddy simulations of a drizzling, stratocumulus-

502 topped marine boundary layer, *Mon. Weather Rev.*, **137(3)**, 1083–1110,

503 *doi:*[10.1175/2008MWR2582.1](https://doi.org/10.1175/2008MWR2582.1).

504 Bony, S., and J.-L. Dufresne (2005), Marine boundary layer clouds at the heart of tropical

505 cloud feedback uncertainties in climate models, *Geophys. Res. Lett.*, **32**, L20806,

506 *doi:*[10.1029/2005GL023851](https://doi.org/10.1029/2005GL023851).

507 Brenguier, J. L., T. Bourriane, A. de Araujo Coelho, R. J. Isbert, R. Peytavi, D.

508 Trevarin, and P. Weschler, 1998: Improvements of droplet distribution size

509 measurements with the fast-FSSP (forward scattering spectrometer probe). *J.*

510 *Atmos. Oceanic Technol.*, **15**, 1077–1090.

511 Bretherton, C. S., and S. Park, 2009: A New Moist Turbulence Parameterization in the

512 Community Atmosphere Model. *J. Climate*, **22**, 3422–3448.

513 Caldwell, P. M., C. S. Bretherton, and R. Wood, 2005: Mixed-Layer Budget Analysis of

514 the Diurnal Cycle of Entrainment in Southeast Pacific Stratocumulus. *J. Atmos.*

515 *Sci.*, **62**, 3775–3791.

516 Doran, J. C., J. M. Hubbe, J. C. Liljegren, W. J. Shaw, G. J. Collatz, D. R. Cook, and R.

517 L. Hart, 1998: A technique for determining the spatial and temporal distributions

518 of surface fluxes of heat and moisture over the Southern Great Plains Cloud and

519 Radiation Testbed, *J. Geophys. Res.*, **103(D6)**, 6109–6121,  
520 *doi:*[10.1029/97JD03427](https://doi.org/10.1029/97JD03427).

521 English, J. M., J. E. Kay, A. Gettelman, X. Liu, Y. Wang, Y. Zhang, and H. Chepfer,  
522 2014: Contributions of clouds, surface albedos, and mixed-phase ice nucleation  
523 schemes to Arctic radiation biases in CAM5, *J. Climate*, **27**, 5174–5197. *doi:*  
524 <http://dx.doi.org/10.1175/JCLI-D-13-00608.1>.

525 Forster, P., Ramaswamy, V., Artaxo, P., Berntsen, T., Betts, R., Fahey, D. W., Haywood,  
526 J., Lean, J., Lowe, D. C., Myhre, G., Nganga, J., Prinn, R., Raga, G., Schulz, M.,  
527 and Dorland, R. V.: Changes in atmospheric constituents and in radiative forcing,  
528 in: *Climate Change 2007: The Physical Science Basis, Contribution of Working*  
529 *Group I to the Fourth Assessment Report of the Intergovernmental Panel on*  
530 *Climate Change*, edited by: Solomon, S., Qin, D., Manning, M., Chen, Z.,  
531 Marquis, M., Averyt, K. B., Tignor, M., and Miller, H. L., Cambridge Univ.  
532 Press, UK and New York, 2007.

533 Frisch, S., M. Shupe, I. Djalalova, G. Feingold, and M. Poellot, 2002: The Retrieval of  
534 Stratus Cloud Droplet Effective Radius with Cloud Radars, *J. Atmos. and Oceanic*  
535 *Tech.* **19**, 835-842.

536 Gettelman, A., H. Morrison, and S. J. Ghan, 2008: A new two-moment bulk stratiform  
537 cloud microphysics scheme in the NCAR Community Atmosphere Model  
538 (CAM3), Part II: Single-column and global results, *J. Climate*, **21(15)**, 3660–  
539 3679.

540 Gettelman, A., X. Liu, S. J. Ghan, H. Morrison, S. Park, A. J. Conley, S. A. Klein, J.  
541 Boyle, D. L. Mitchell, and J.-L. F. Li (2010), Global simulations of ice nucleation  
542 and ice supersaturation with an improved cloud scheme in the Community  
543 Atmosphere Model, *J. Geophys. Res.*, **115**, D18216, doi:10.1029/2009JD013797.

544 Gettelman, A., X. Liu, D. Barahona, U. Lohmann, and C. Chen, 2012: Climate impacts of  
545 ice nucleation, *J. Geophys. Res.*, **117**, D20201, doi:10.1029/2012JD017950.

546 Gettelman, A., H. Morrison, S. Santos, P. Bogenschutz and P. M. Caldwell, 2014:  
547 Advanced Two-Moment Microphysics for Global Models. Part II: Global model  
548 solutions and Aerosol-Cloud Interactions., *J. Climate*, in press,  
549 [http://www.cgd.ucar.edu/staff/andrew/papers/gettelman\\_mg2\\_global\\_rev2.pdf](http://www.cgd.ucar.edu/staff/andrew/papers/gettelman_mg2_global_rev2.pdf)

550 Ghan, S. J., et al., 2000, A comparison of single column model simulations of  
551 summertime midlatitude continental convection, *J. of Geophys. Res.*, **105**, 2091-  
552 2124.

553 Ghan, S. J. , X. Liu, R. C. Easter, R. Zaveri, P. J. Rasch, J.-H. Yoon, and B. Eaton, 2012:  
554 Toward a Minimal Representation of Aerosols in Climate Models: Comparative  
555 Decomposition of Aerosol Direct, Semidirect, and Indirect Radiative Forcing. *J.*  
556 *Climate*, **25**, 6461–6476. doi: <http://dx.doi.org/10.1175/JCLI-D-11-00650.1>

557 Hack, J. J., and J. A. Pedretti, 2000: Assessment of Solution Uncertainties in Single-  
558 Column Modeling Frameworks. *J. Climate*, **13**, 352–365. doi:  
559 [http://dx.doi.org/10.1175/1520-0442\(2000\)013<0352:AOSUIS>2.0.CO;2](http://dx.doi.org/10.1175/1520-0442(2000)013<0352:AOSUIS>2.0.CO;2)

560 Hannay, C., D. L. Williamson, J. J. Hack, J. T. Kiehl, J. G. Olson, S. A. Klein, C. S.  
561 Bretherton, and M. Koehler, 2009: Evaluation of forecasted Southeast Pacific

562 stratocumulus in the NCAR, GFDL and ECMWF models. *J. Climate*, **22**, 2871-  
563 2889.

564 Hartmann, D. L., M. E. Ockert-Bell, and M. L. Michelsen, 1992: The Effect of Cloud  
565 Type on Earth's Energy Balance: Global Analysis. *J. Climate*, **5**, 1281–1304.

566 Haywood, J. M., and Boucher, O., 2000: Estimates of the direct and indirect radiative  
567 forcing due to tropospheric aerosols, 2000: A review, *Rev. Geophys.*, **38**, 513–  
568 543, doi: 10.1029/1999RG000078.

569 Iacobellis, S. F., and R. C. J. Somerville, 2006: Evaluating parameterizations of  
570 the autoconversion process using a single-column model and  
571 Atmospheric Radiation Measurement Program measurements, *J.*  
572 *Geophys. Res.*, **111**, D02203, doi:10.1029/2005JD006296.

573 Klein, S.A., et al., 2009: Intercomparison of model simulations of mixed-phase clouds  
574 observed during the ARM Mixed-Phase Arctic Cloud Experiment. Part I: Single-  
575 layer cloud., *Q. J. R. Meteorol. Soc.*, **135**, no. 641, 979-1002, doi:10.1002/qj.416.

576 Liu, X., S. Xie, J. Boyle, S. A. Klein, X. Shi, Z. Wang, W. Lin, S. J. Ghan, M. Earle, P. S.  
577 K. Liu, Z. Wang and A. Zelenyuk, 2011: Testing cloud microphysics  
578 parameterizations in NCAR CAM5 with ISDAC and M-PACE observations, *J.*  
579 *Geophys. Res.*, **116**, D00T11, doi:10.1029/2011JD015889.

580 Liu, X., et al., 2012: Towards a minimal representation of aerosol direct and indirect  
581 effects: Model description and evaluation, *Geosci. Model Dev.*, **5**, 709–735,  
582 doi:10.5194/gmd-4-709-2012.

583 Martin, G. M., D. W. Johnson, and A. Spice, 1994: The Measurement and  
584 Parameterization of Effective Radius of Droplets in Warm Stratocumulus Clouds,  
585 *J. Atmos. Sci.*, **51**, 1823–1842.

586 Medeiros B., B. Stevens, I. M. Held, M. Zhao, D. L. Williamson, J. G. Olson, and C. S.  
587 Bretherton, 2008: Aquaplanets, Climate Sensitivity, and Low Clouds. *J. Climate*,  
588 **21**, 4974–4991.

589 Meyers, M. P., P. J. DeMott, and W. R. Cotton, 1992: New primary ice-nucleation  
590 parameterizations in an explicit cloud model, *J. Appl. Meteorol.*, **3**, 708–721.

591 Mlawer, E. J., S. J. Taubman, P. D. Brown, M. J. Iacono, and S. A. Clough, 1997:  
592 Radiative transfer for inhomogeneous atmosphere: RRTM, a validated correlated-  
593 k model for the longwave, *J. Geophys. Res.*, **102 (D14)**, 16 663–16 682.

594 Moeng, C., H., W. R. Cotton, C. S. Bretherton, A. Chlond, M. Khairoutdinov, S.  
595 Krueger, W. S. Lewellen, M. K. MacVean, J. R. M. Pasquier, H. A. Rand, A. P.  
596 Siebesma, R. I Sykes, and B. Stevens, 1996: Simulation of a stratocumulus-  
597 topped PBL: Intercomparison among different numerical codes, *Bull. Amer.*  
598 *Meteorol. Soc.*, **77**, 261–27.

599 Morrison H, and Gettelman A., 2008: A new two-moment bulk stratiform cloud  
600 microphysics scheme in the Community Atmosphere Model, version 3 (CAM3).  
601 Part I: Description and numerical tests, *J. Climate*, **21**, 3642–3659.

602 Neale, R., and Coauthors, 2012: Description of the NCAR Community Atmosphere  
603 Model (CAM 5.0). NCAR Tech. Note NCAR-TN-486+STR, 274 pp.

604 Park, S., and C. S. Bretherton, 2009: The University of Washington Shallow Convection  
605 and Moist Turbulence Schemes and Their Impact on Climate Simulations with the  
606 Community Atmosphere Model, *J. Climate*, **22**, 3449–3469.  
607 doi:<http://dx.doi.org/10.1175/2008JCLI2557.1>

608 Park, S., C. S. Bretherton, and P. J. Rasch, 2014: Integrating Cloud Processes in the  
609 Community Atmosphere Model, Version 5, *J. Climate*, **27**, 6821–6856.  
610 doi: <http://dx.doi.org/10.1175/JCLI-D-14-00087.1>  
611

612 Randall, D., S. Krueger, C. Bretherton, J. Curry, Duynkerke, M. Moncireff, B. Ryan, D.  
613 Starr, M. Miller, W. Rossow, G. Tselioudis, and B. Wielicki, 2003: Confronting  
614 models with data: The GEWEX Cloud Systems Study. *Bull. Amer. Meteorol.*  
615 *Soc.*, **84**, 455-469, doi:10.1175/BAMS-84-4-455.

616 Rauber, R. M., et al., 2007: Rain in Shallow Cumulus Over the Ocean: The RICO  
617 campaign, *Bull. Am. Meteorol. Soc.*, **88 (12)**, 1912–1928.

618 J. H. Richter and P. J. Rasch, 2008: Effects of Convective Momentum Transport on the  
619 Atmospheric Circulation in the Community Atmosphere Model, Version 3. *J.*  
620 *Climate*, **21**, 1487–1499.

621 Schubert, W. H., J. S. Wakefield, E. J. Steiner, and S. K. Cox (1979b), Marine  
622 stratocumulus convection. Part I: Governing equations and horizontally  
623 homogeneous solutions, *J. Atmos. Sci.*, **36(7)**, 1286–1307.

624 Siebesma, A. P., and Coauthors, 2003: A large eddy simulation intercomparison study of  
625 shallow cumulus convection, *J. Atmos. Sci.*, **60**, 1201–1219.

626 Sobel, A. H. and C. S. Bretherton, 2000: Modeling Tropical Precipitation in a Single  
627 Column. *J. Climate*, **13**, 4378–4392.

628 Stevens, B, Moeng C-H, Ackerman AS, Bretherton CS, Chlond A, de Roode S, Edwards  
629 J, Golaz J-C, Jiang H, Khairoutdinov M, Kirkpatrick MP, Lewellen DC, Lock A,  
630 Muller F, Stevens DE, Whelan E, Zhu P., 2005: Evaluation of large-eddy  
631 simulations via observations of nocturnal marine stratocumulus, *Mon. Weather*  
632 *Rev.*, **133**, 1443–1462.

633 vanZanten, M. C., and Coauthors, 2011: Controls on precipitation and cloudiness in  
634 simulations of trade-wind cumulus as observed during RICO, *J. Adv. Model.*  
635 *Earth Syst.*, **3**, M06001, doi:10.1029/2011MS000056.

636 Wyant, M. C. et al., 2007: A single-column model intercomparison of a heavily drizzling  
637 stratocumulus-topped boundary layer, *J. Geophys. Res.*, **112**, D24204,  
638 doi:10.1029/2007JD008536.

639 Xie, S., X. Liu, C. Zhao, and Y. Zhang (2013), Sensitivity of CAM5 simulated Arctic  
640 clouds and radiation to ice nucleation parameterization, *J. Climate*, **26**, 5981–  
641 5999, doi: <http://dx.doi.org/10.1175/JCLI-D-12-00517.1>.

642 Xu, K., -M, and D. A. Randall, 2000: Explicit Simulation of Midlatitude Cumulus  
643 Ensembles: Comparison with ARM Data. *J. Atmos. Sci.*, **57**, 2839–2858. doi:  
644 [http://dx.doi.org/10.1175/1520-0469\(2000\)057<2839:ESOMCE>2.0.CO;2](http://dx.doi.org/10.1175/1520-0469(2000)057<2839:ESOMCE>2.0.CO;2)

645 Zhang, G. J., and N. A. McFarlane, 1995: Sensitivity of climate simulate simulation to  
646 the parameterization of cumulus convection in the Canadian Climate center  
647 general circulation model, *Atmos. Ocean*, **33**, 407-446.

648 Zhang, M. H., J. L. Lin, R. T. Cederwall, J. J. Yio, and S. C. Xie, 2001: Objective  
649 analysis of ARM IOP Data: Method and sensitivity, *Mon. Weather Rev.*, **129**,  
650 295-311.

651 Zhu, P., and Coauthors, 2005: Intercomparison and Interpretation of Single-Column  
652 Model Simulations of a Nocturnal Stratocumulus-Topped Marine Boundary  
653 Layer. *Mon. Wea. Rev.*, **133**, 2741–2758. doi: [http://dx.doi.org/10.1175/  
654 MWR2997.1](http://dx.doi.org/10.1175/MWR2997.1)

655  
656  
657  
658  
659  
660  
661

Table 1: Initial and boundary conditions for DYCOMS RF02, MPACE-B, and RICO cases. All heights  $z$  are in meters and all pressures  $p$  are in hPa. Boundary layer height and vertical velocity are (respectively)  $z_i$  and  $w$  in height coordinates and  $p_i$  and  $\omega$  in pressure coordinates. N/A indicates a quantity which is not used or is calculated by the model itself.  $q_t$  is total water mixing ratio,  $\theta$  is potential temperature, and  $\theta_l$  is liquid water potential temperature. One of the 3 aerosol modes for each case is omitted because it has zero mass.

	<i>DYCOMS RF02</i>	<i>MPACE-B</i>	<i>RICO</i>
run time (hrs):	6	12	24
SHF ( $\text{W m}^{-2}$ ):	93	136.5	N/A
LHF ( $\text{W m}^{-2}$ ):	16	107.7	N/A
$u$ ( $\text{m s}^{-1}$ ):	$3 + 4.3z/1000$	-13	$-1.9-8 \min(z, z_i)/z_i$
$v$ ( $\text{m s}^{-1}$ ):	$-9 + 5.6 z/1000$	-3	-3.8
vert veloc:	$w = -3.75 \times 10^{-6} z$ ( $\text{m s}^{-1}$ )	$\omega = 80 \min(p, p_i)/p_i$ ( $\text{mb day}^{-1}$ )	$w = -0.5 \min(z, 2260)/2260$ ( $\text{m s}^{-1}$ )
Large-scale $q_t$ tend ( $\text{g kg}^{-1} \text{day}^{-1}$ ):	0	$\min\{-0.164, -3[1 - (p_s - p)/151.71]\}$	$-1+1.3456 \min\{z, 2980\}/2980$
Large-scale $T$ tend ( $\text{K day}^{-1}$ ):	0	$\min\{-4, -15[1 - (p_s - p)/218.18]\}$	-2.5
init $q_t$ ( $\text{g kg}^{-1}$ ):	$9.45 \text{ g kg}^{-1}$ if $z < z_i$ , else $5 - 3(1 - e^{(z_i - z)/500})^{1/3}$	$1.95$ if $p > p_i$ , else $0.291 + 0.00204(p - 590)$	$16 - 2.2 z/740$ if $z < 740$ , $13.8 - 11.4(z - 740)/2520$ if $740 < z < 3260$ $2.4 - 0.6(z - 3260)/740$ else
init $\theta_l$ (K):	$288.3 \text{ K}$ if $z < z_i$ , else $295 + (z - z_i)^{1/3}$	$269.2$ if $p > p_i$ , else $275.33 + 0.0791(815 - p)$	$297.9$ if $z < 740$ , else $297.9 + 19.1(z - 740)/(4000 - 740)$
<i>For FixHydro</i> $N_d$ ( $\# \text{ cm}^{-3}$ ): $N_i$	55 N/A	50 $0.16 \text{ L}^{-1}$	70 N/A
<i>For ObsAero</i> <i>Mode:</i> compos: # concentr : mode radius: geometric $\sigma$ : <i>Mode:</i> compos: # concentr: mode radius: geometric $\sigma$ :	Aitken 100% SO <sub>4</sub> $125 \text{ cm}^{-3}$ $0.011 \mu\text{m}$ 1.2 Accumulation 100% SO <sub>4</sub> $65 \text{ cm}^{-3}$ $0.06 \mu\text{m}$ 1.7	Accumulation 70% SO <sub>4</sub> , 30% particulate organic matter $72.2 \text{ cm}^{-3}$ $0.052 \mu\text{m}$ 2.04 Coarse 10% SO <sub>4</sub> , 85% sea salt, 5% dust $1.8 \text{ cm}^{-3}$ $1.3 \mu\text{m}$ 2.5	Aitken 100% SO <sub>4</sub> $90 \text{ cm}^{-3}$ $0.03 \mu\text{m}$ 1.28 Accumulation 100% SO <sub>4</sub> $150 \text{ cm}^{-3}$ $0.14 \mu\text{m}$ 1.75

662

663 Table 2: Data averaged over the last two hours of the DYCOMS RF02 simulations.  
 664 Observations are from W07.  $N_d$  is the average over the in-cloud portion of all cloudy  
 665 levels of the column.

	$N_d$ ( $\text{cm}^{-3}$ )	$LWP_{\text{pre}}$ ( $\text{g m}^{-2}$ )	$LWP_{\text{post}}$ ( $\text{g m}^{-2}$ )	$w_e$ ( $\text{mm s}^{-1}$ )	$z_b$ (m)	$z_i$ (m)	Surf Pr (mm/day)
Obs	55	80-120	80-120	6-7.6	~450	~800	0.35
Default	33	103	73	4.2	475	803	0.31
PrescAero	139	137	126	4.0	473	816	0.04
ObsAero	74	146	119	3.4	492	815	8.5e-6
FixHydro	55	174	145	3.6	465	818	6.9e-6

666

667

668

669 Table 3: As in Table 2, but for MPACE-B using the last 4 simulated hours. Observations  
 670 are from K09.

	$N_i$ ( $\text{L}^{-1}$ ), $N_d$ ( $\text{cm}^{-3}$ )	$LWP$ ( $\text{g m}^{-2}$ )	$IWP$ ( $\text{g m}^{-2}$ )	$w_e$ ( $\text{mm s}^{-1}$ )	$z_b$ (m)	$z_i$ (m)	Surf Pr (mm/day)
Obs	0.16,50	110-210	8-30	-	~600	~1500	0.25
Default	0.4,0	3.96e-9	0.022	11.46	918	1476	0.82
PrescAero	0.7,0	3.69e-9	0.018	15.37	984	1537	0.69
ObsAero	0.6,0	3.64e-9	0.014	15.37	985	1537	0.68
FixHydro	0.16,50	133	0.63	12.37	872	1783	0.50

671

672

673

674 Table 4: Data averaged over the last four 4 hrs of RICO runs. LES data are from VZ11.

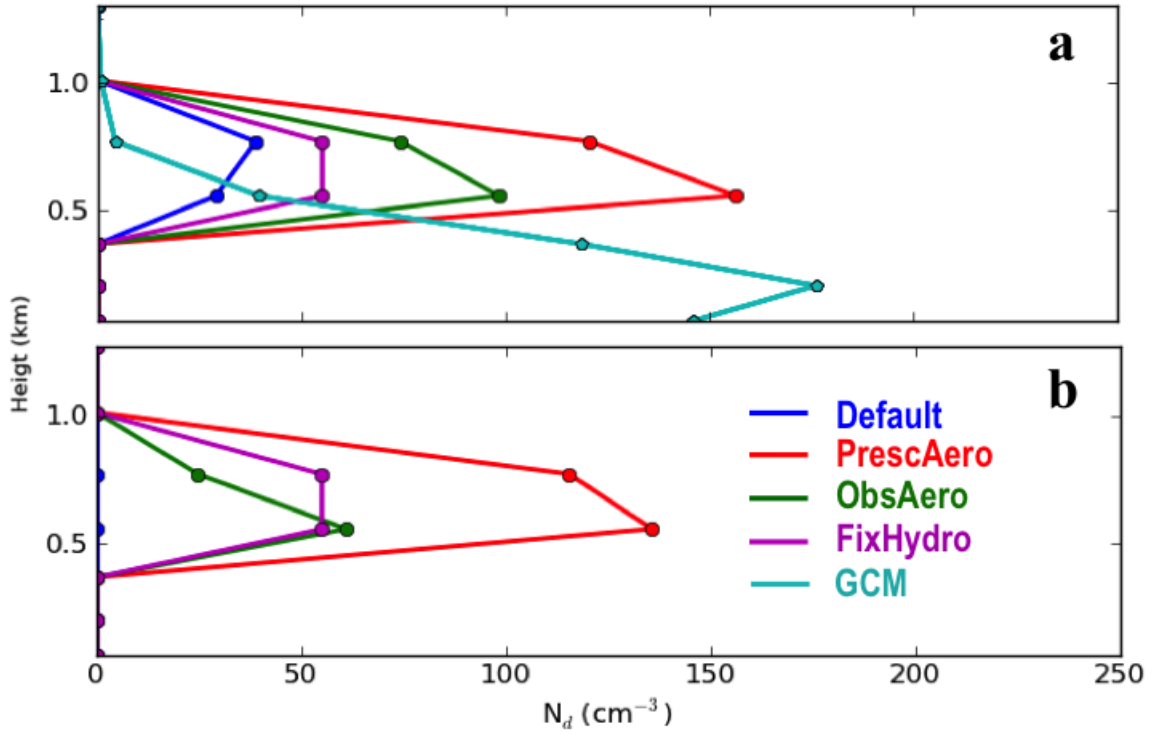
	$N_d$ ( $\text{cm}^{-3}$ )	SHF ( $\text{w m}^{-2}$ )	LHF ( $\text{wm}^{-2}$ )	CBMF ( $\text{m s}^{-1}$ )	Cloud Cover	<sup>675</sup> <del>LWP</del> <sup>676</sup> ( $\text{g m}^{-2}$ )
LES	70	8.5	158	0.026	0.19	<sup>677</sup> 19.6
Default	30	12.29	207.81	0.06	0.18	<sup>678</sup> 19.0
PrescAero	32	12.41	207.94	0.06	0.18	<sup>679</sup> 19.2
ObsAero	14	12.42	207.83	0.06	0.18	19.8
FixHydro	70	12.37	207.83	0.06	0.18	19.6

680 **Figure Captions**

681

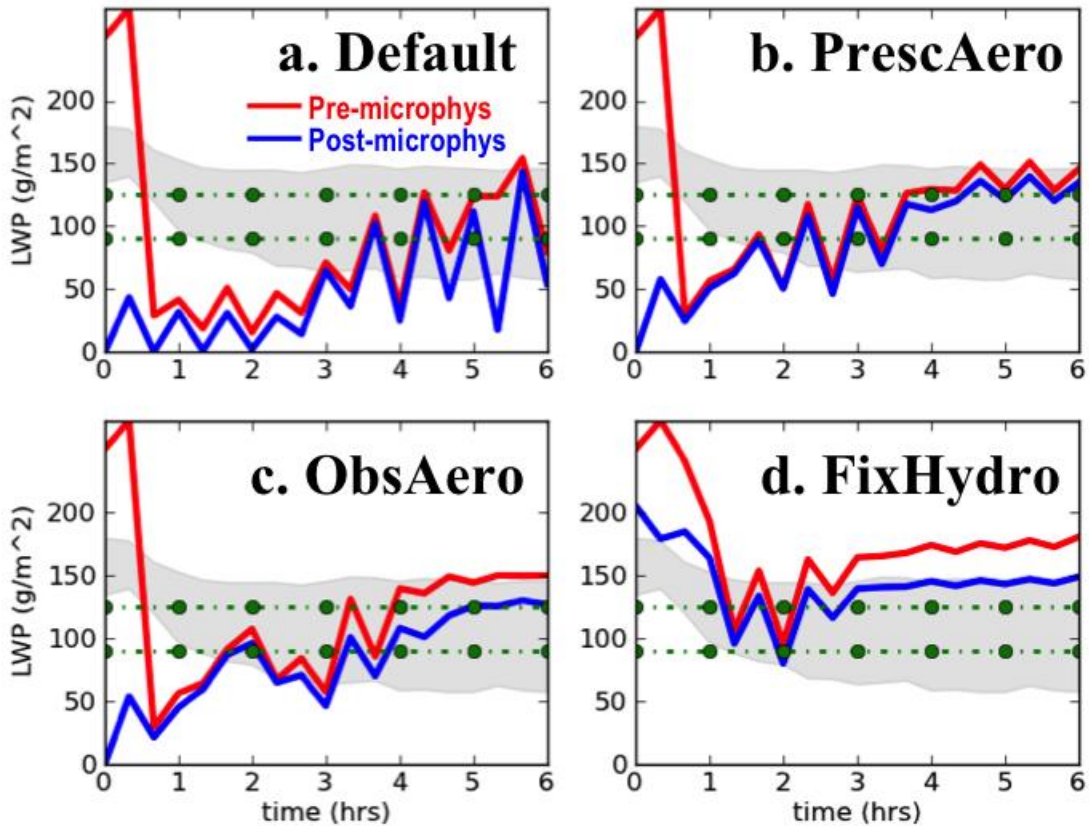
- 682 1. Profiles of in-cloud droplet number concentrations ( $N_d$ ) for DYCOMS RF02. GCM  
683 values are July climatologies extracted from a 10-yr long prognostic aerosol GCM  
684 run at the location of DYCOMS RF02. Panel a is for runs where condensate is  
685 detrained (the default model behavior) and panel b shows runs where all detrained  
686 water is in vapor phase.
- 687 2. Time series of LWP before and after microphysics for DYCOMS RF02. The shaded  
688 area indicates the range of LES values averaged over the last 4hrs of the simulation  
689 period from Stevens and Seifert (2008) and the area bounded by dots indicates the  
690 range of observational uncertainty from Stevens et al. (2003).
- 691 3. LWC and IWC profiles as a function of scaled height ( $z/z_b-1$ ) for MPACE-B. Dashed  
692 lines indicate values before microphysics and solid lines indicate values after  
693 microphysics. a) LWC profiles as function of scaled height. Dark shaded region  
694 ranges, light shaded region and black solid line depict the median value, the inner  
695 50% and the outer 50% the envelope of the high frequency observed aircraft data  
696 respectively (from K09). b) the same as figure 3a but for IWC (including snow). c)  
697 same as figure 6b but using radar data from K09 as observations. d) same as figure 3b  
698 but excluding snow.
- 699 4. Profiles of in-cloud  $N_i$  values for MPACE-B. GCM values are 10 year July averages  
700 extracted at the location of MPACE-B divided by 10 in order to fit in the plot.
- 701 5. Time-averaged profiles of cloud fraction from models and observations as a function  
702 of height during the MPACE-B period. All observations are taken from K09.
- 703 6. Time series of LWP during the RICO IOP period. LES data comes from VZ11.
- 704 7. Time-averaged profiles of a) condensate amount and b) mass-flux for RICO  
705 simulations. The colored line shows the SCM results (all simulations lie on top of one  
706 another). Shading in figure 8b indicates ensemble inter quartile range and the solid  
707 black line is the ensemble mean. LES data are from VZ11.
- 708 8. Time-averaged profiles cloud fraction (CF) quantities from RICO simulations.  
709 Default, PrescAero, and ObsAero all lie on top of one another. LES data are from  
710 VZ11.
- 711 9. Time series of: a) LWP and b) IWC during the ARM95 IOP period. The solid black  
712 line in panel a) gives observations from Xu and Randall (2000).
- 713 10. Profiles of in-cloud droplet number concentrations ( $N_d$ ) during the ARM95 IOP  
714 period. Blue=Default case and Red= PrescAero case; Cyan= 10 years July average  
715 default global CAM extracted at the location of ARM95; Yellow= 10 years July  
716 average PrescAero global CAM extracted at the location of ARM95.

717



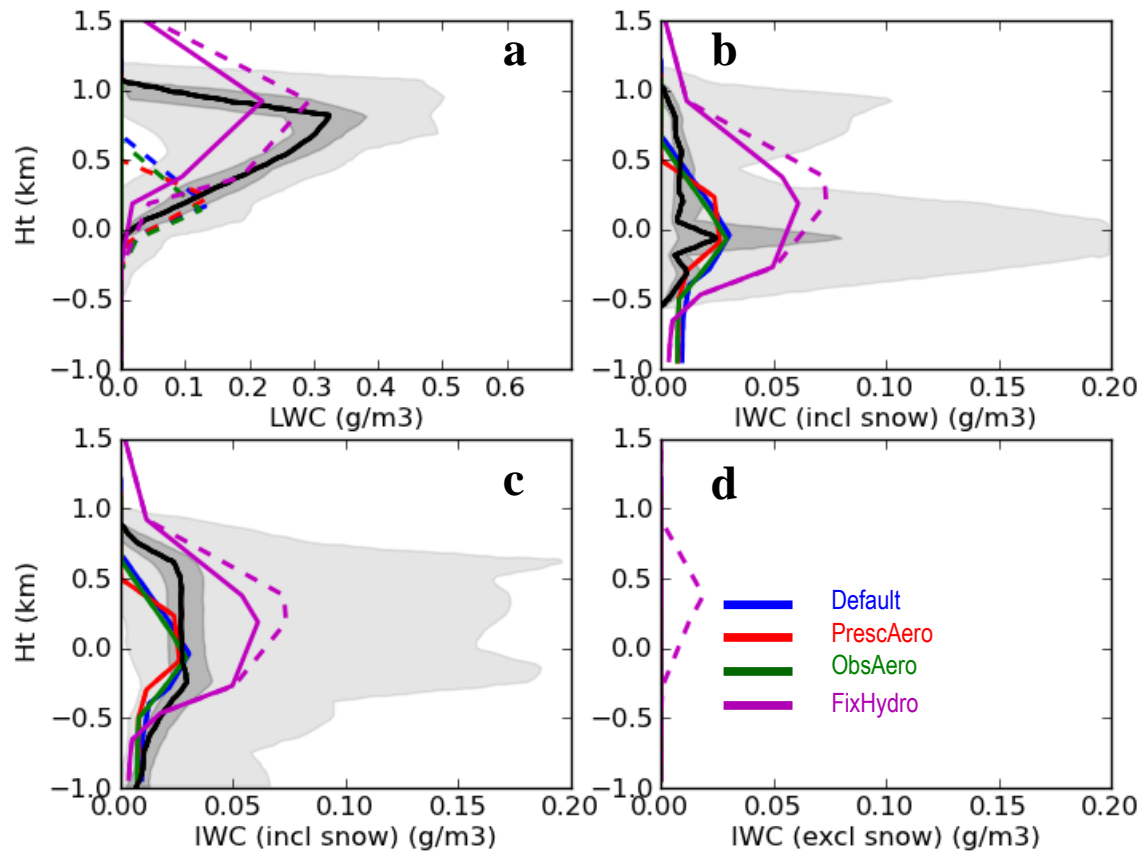
718  
 719 11. Figure 1: Profiles of in-cloud droplet number concentrations ( $N_d$ ) for DYCOMS  
 720 RF02. GCM values are July climatologies extracted from a 10-yr long prognostic  
 721 aerosol GCM run at the location of DYCOMS RF02. Panel a is for runs where  
 722 condensate is detrained (the default model behavior) and panel b shows runs where  
 723 all detrained water is in vapor phase.  
 724

725  
726  
727  
728



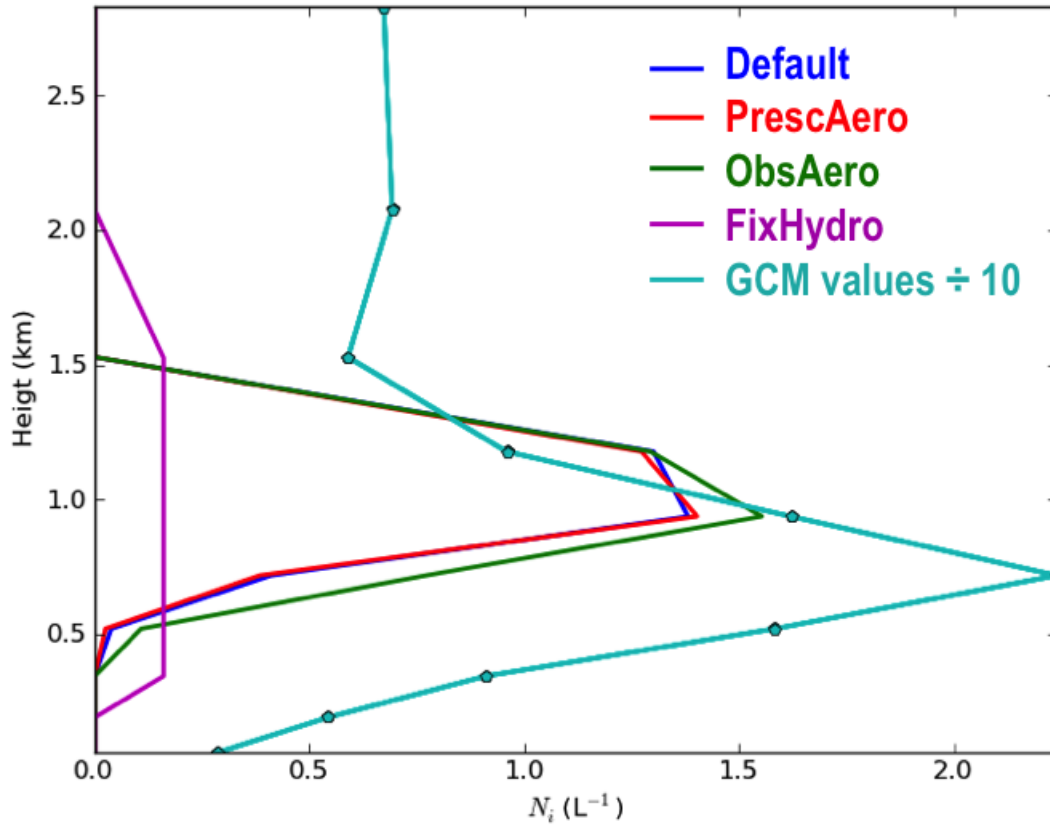
729  
730  
731  
732  
733  
734  
735  
736

Figure 2. Time series of LWP before and after microphysics for DYCOMS RF02. The shaded area indicates the range of LES values averaged over the last 4hrs of the simulation period from Stevens and Seifert (2008) and the area bounded by dots indicates the range of observational uncertainty from Stevens et al. (2003).



737 Figure 3. LWC and IWC profiles as a function of scaled height ( $z/z_b-1$ ) for MPACE-B.  
 738 Dashed lines indicate values before microphysics and solid lines indicate values after  
 739 microphysics. a) LWC profiles as function of scaled height. Dark shaded region ranges,  
 740 light shaded region and black solid line depict the median value, the inner 50% and the  
 741 outer 50% the envelope of the high frequency observed aircraft data respectively (from  
 742 K09). b) the same as figure 3a but for IWC (including snow). c) same as figure 6b but  
 743 using radar data from K09 as observations. d) same as figure 3b but excluding snow.  
 744  
 745  
 746

747



748

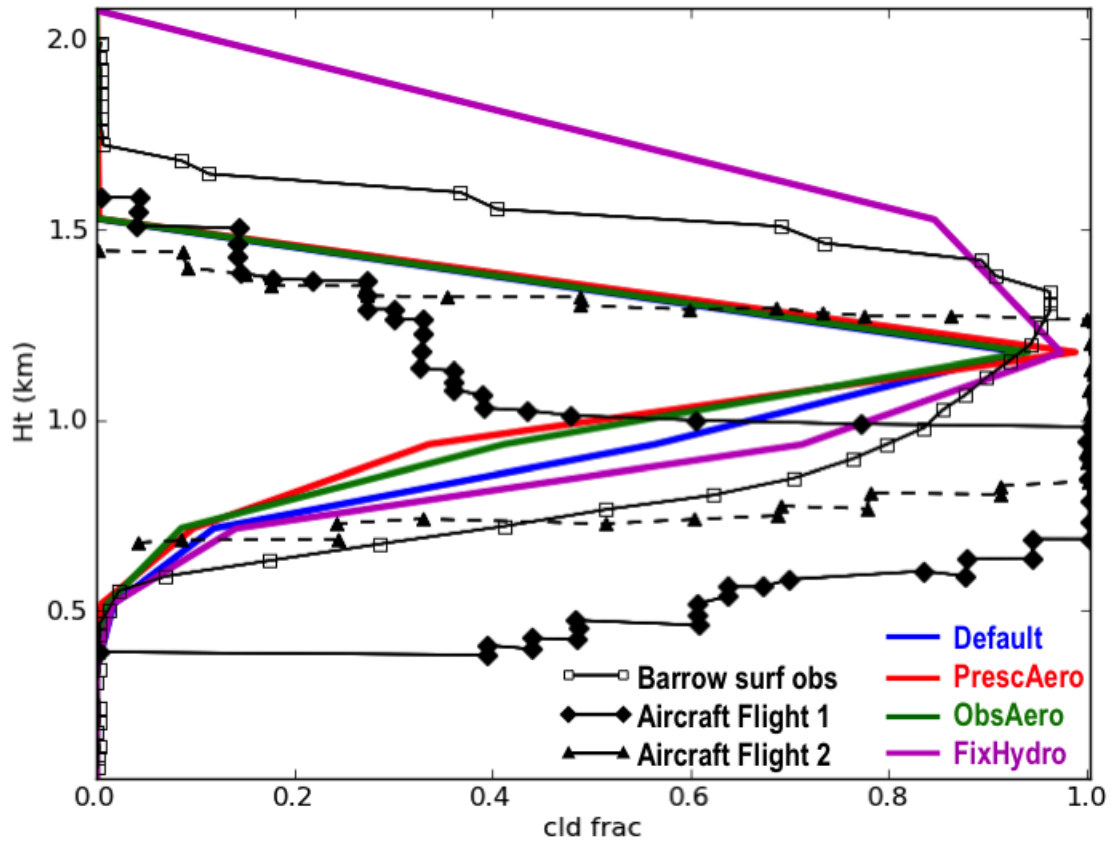
749

750 Figure 4. Profiles of in-cloud  $N_i$  values for MPACE-B case. GCM values are 10 year July

751 averages extracted at the location of MPACE-B divided by 10 in order to fit in the plot.

752

753

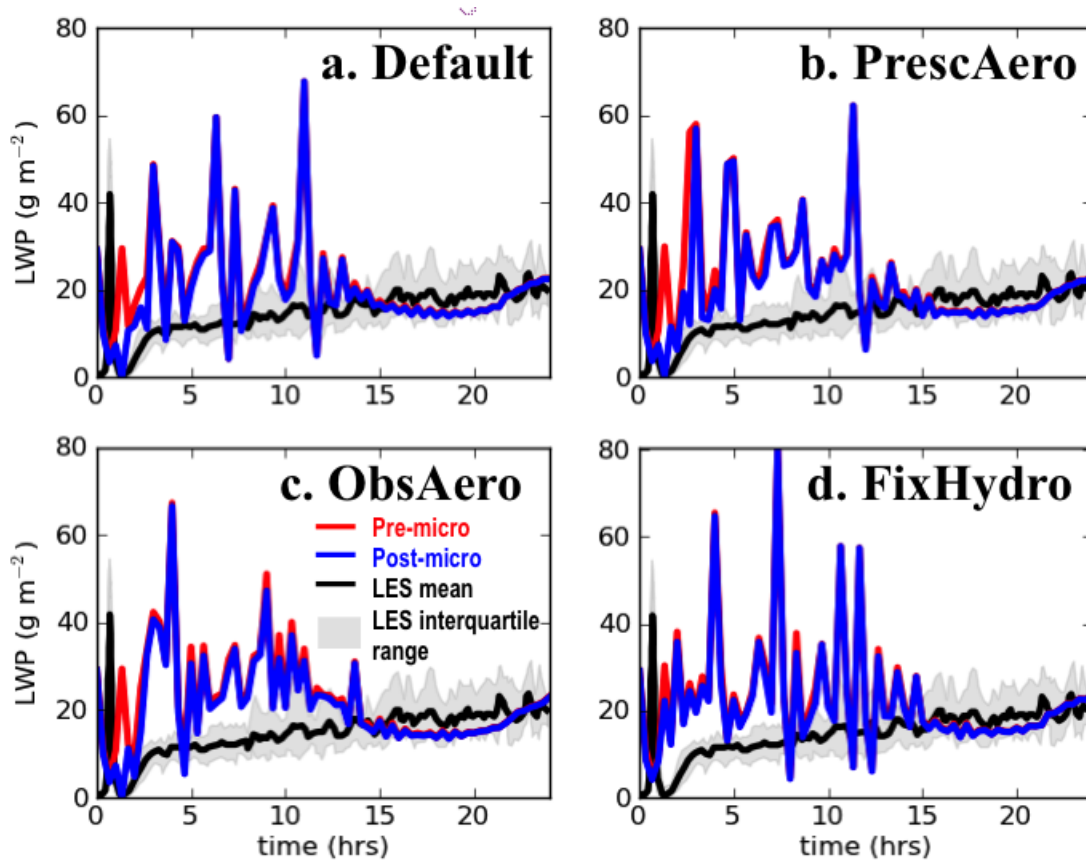


754

755 Figure 5. Time-averaged profiles of cloud fraction from models and observations as a  
756 function of height during the MPACE-B period. All observations are taken from K09.

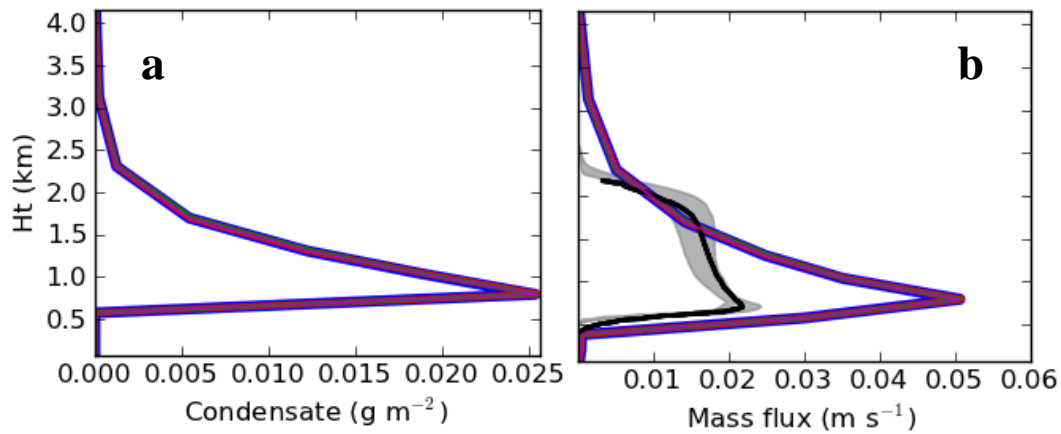
757

758



759  
 760  
 761  
 762  
 763

Figure 6. Time series of LWP during the RICO IOP period. LES data comes from VZ11.

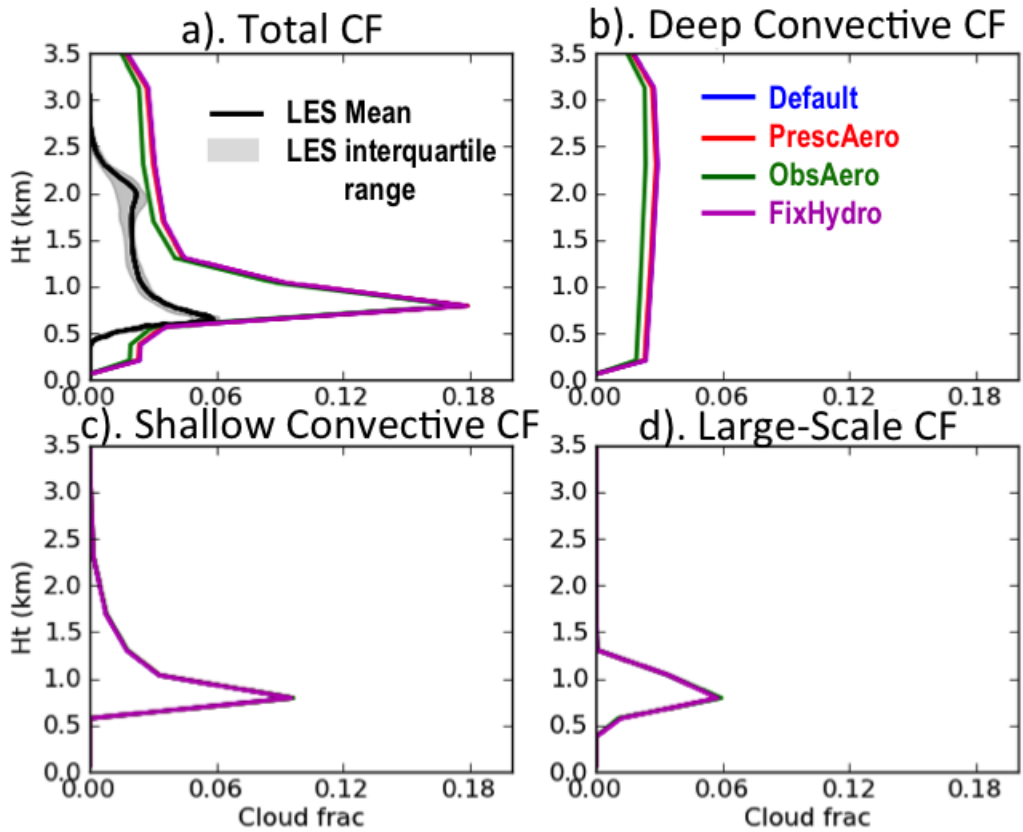


777

778 Figure 7. Time-averaged profiles of a) condensate amount and b) mass-flux for RICO  
779 simulations. The colored line shows the SCM results (all simulations lie on top of one  
780 another). Shading in figure 8b indicates ensemble inter quartile range and the solid black  
781 line is the ensemble mean. LES data are from VZ11.

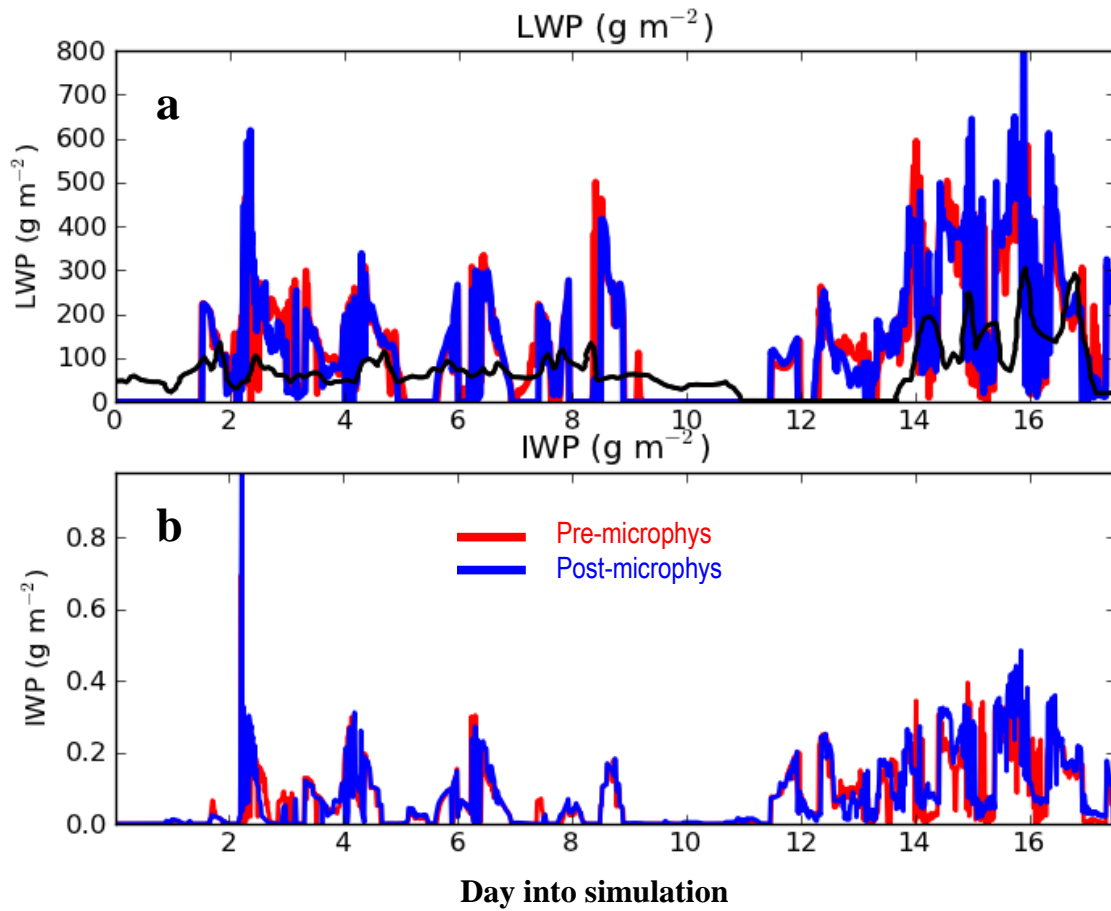
782

783



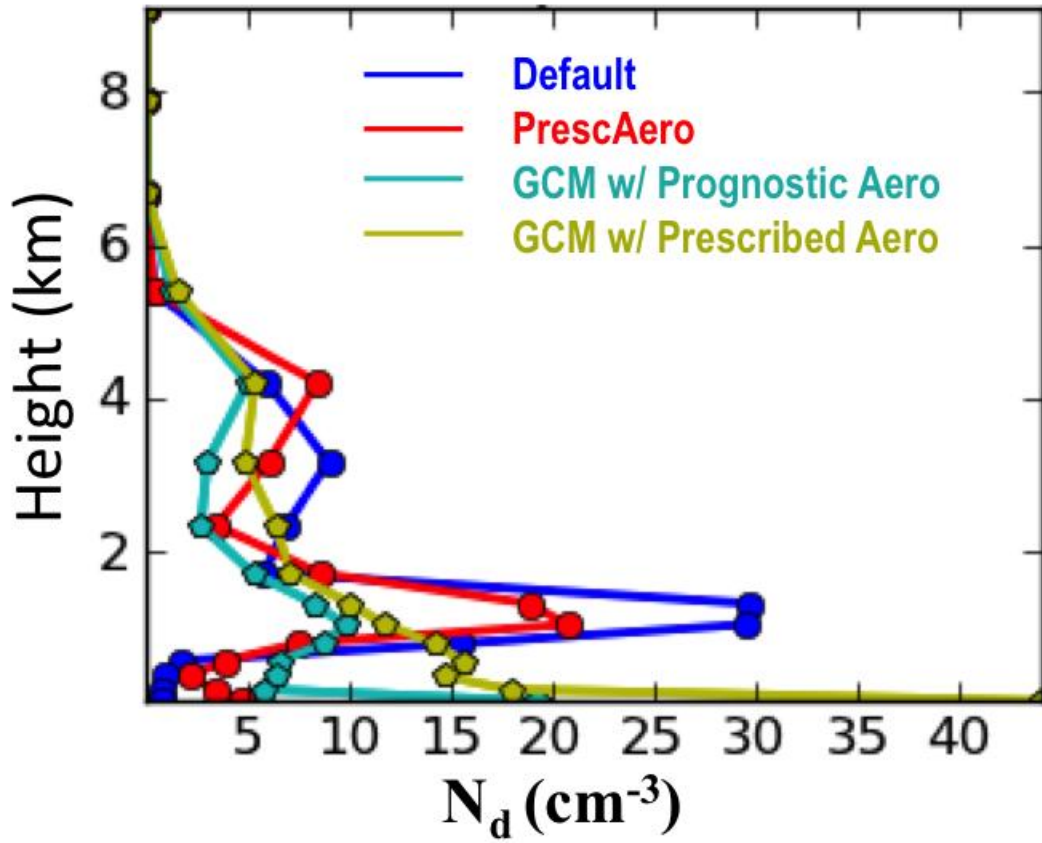
784  
 785  
 786  
 787  
 788

Figure 8. Time-averaged profiles cloud fraction (CF) quantities from RICO simulations. Default, PrescAero, and ObsAero all lie on top of one another. LES data are from VZ11.



789  
 790  
 791  
 792

Figure 9. Time series of: a) LWP and b) IWP during the ARM95 IOP period. The solid black line in panel a) gives observations from Xu and Randall (2000).



793  
 794  
 795  
 796  
 797  
 798  
 799  
 800  
 801  
 802

Figure 10. Profiles of in-cloud droplet number concentrations ( $N_d$ ) during the ARM95 IOP period. GCM results are climatological July averages extracted at the location of ARM95.